PCCP

Accepted Manuscript

ROYAL SOCIETY OF CHEMISTRY

www.rsc.org/pccp

Journal Name

RSC Publishing

ARTICLE

Highly efficient exciton harvesting and charge transport in ternary blend solar cells based on wide- and low-bandgap polymers

Yanbin Wang,[a,b] Hideo Ohkita,*[a,c] Hiroaki Benten,[a] and Shinzaburo Ito[a]

Cite this: DOI: 10.1039/x0xx00000x

Received ooth January 2012,
Accepted ooth January 2012

DOI: 10.1039/x0xx00000x

www.rsc.org/

We have designed highly efficient ternary blend solar cells based on a wide-bandgap crystalline polymer, poly(3-hexylthiophene) (P3HT), and a low-bandgap polymer, poly[(4,4'-bis(2-ethylhexyl)dithieno[3,2-b:2'3'-d]silole)-2,6-diyl-*alt*-(2,1,3-benzothiadiazole)-4,7-diyl] (PSBTBT), and a fullerene derivative (PCBM). By using highly crystalline P3HT, high fill factors were obtained even for ternary blend solar cells, suggesting efficient charge transport due to large P3HT crystalline domains. In such large crystalline domains, some P3HT excitons could not diffuse into the interface to PCBM but can be collected to PSBTBT domains by efficient energy transfer because of large spectral overlap between the P3HT fluorescence and the PSBTBT absorption. Consequently, all the P3HT excitons can contribute to the photocurrent generation at the P3HT/PCBM interface and/or PSBTBT domains mixed with PCBM in the ternary blends. As a result, P3HT/PSBTBT/PCBM ternary blend solar cells exhibit a power conversion efficiency of 5.6%, which is even higher than that of both individual binary devices of P3HT/PCBM and PSBTBT/PCBM.

Introduction

Polymer solar cells based on binary blends of polymeric donor and fullerene acceptor materials have been extensively investigated in the past decade.[1–5] The power conversion efficiency (PCE) has been improved every year and very recently exceeded 10% by several groups.[6–10] However, it is still not high enough to compete with commercialized inorganic solar cells.[6] One of the most important reasons is the spectral mismatch between an absorption band of the photoactive layer and the terrestrial solar radiation.[11] For example, poly(3-hexylthiophene) (P3HT) exhibits a large absorption band in the visible region from 400 to 600 nm but no absorption band in the near-IR region. As a result, the PCE of polymer solar cells based on a blend of P3HT and a fullerene derivative (PCBM) is limited to less than 5%, even though the external quantum efficiency (EQE) is as high as 80%.[12,13] Therefore, many more photons not only in the visible region but also in the near-IR region should be absorbed to improve the efficiency furthermore.

Ternary blend solar cells have been proposed as a simple and versatile alternative approach to extending the light-harvesting range up to the near-IR region.[14–18] More specifically, ternary blend solar cells are classified into two types. One is dye-sensitized polymer/fullerene solar cells, which are incorporated with dye molecules with complementary absorption bands.[19–32] The other is ternary blends based on an acceptor fullerene and two donor polymers with complementary absorption bands.[33–53] For dye-sensitized ternary blend polymer solar cells, the device performance is higher than that of the original binary solar cells because of the additional dye absorption and the improved exciton harvesting. For two-donor ternary blend polymer solar cells, the device performance is higher than that of the original binary solar cells with a wide-bandgap polymer. In most cases, however, it is still comparable to or lower than that of the original binary solar cells with a low-bandgap polymer after appropriate optimizations,[38,40,41,43-45,51,54–58] suggesting that there are some limitations for this ternary solar cell. This is partly because the light absorption is enhanced in the near-IR region but reduced in the visible region with increasing fraction of the low-bandgap polymer and partly because a fill factor (FF) is degraded with increasing fraction of the low-bandgap polymer.[38,40,43,44,51,59]

Herein, we have fabricated ternary blend solar cells based on wide- and low-bandgap polymers and PCBM. To overcome the limitations mentioned above, we have employed highly crystalline P3HT as a wide-bandgap polymer and poly[(4,4'-bis(2-ethylhexyl)dithieno[3,2-b:2'3'-d]silole)-2,6-diyl-*alt*-(2,1,3-benzothiadiazole)-4,7-diyl] (PSBTBT) as a low-bandgap polymer, which have complementary absorption bands in the visible and in the near-IR region, respectively. Highly crystalline P3HT is likely to form large crystalline domains, which would improve charge transport even in ternary blends. The

complementary absorption bands can extend the light-harvesting range from visible to near-IR region and also give large spectral overlap between the P3HT fluorescence and the PSBTBT absorption, which would improve exciton harvesting by efficient energy transfer from P3HT to PSBTBT even in large P3HT crystalline domains. On the basis of these strategies, high short-circuit current density (J_{SC}) and high FF were obtained at the same time, resulting in an improved PCE of 5.6%, which is even higher than that of both individual binary solar cells based on P3HT/PCBM and PSBTBT/PCBM reported so far.[54,55,60] In order to discuss how P3HT crystallization impacts on the photovoltaic performance of ternary blend solar cells, we have employed two different P3HT with a regioregularity of >98% (P3HT-H) and 85% (P3HT-L).

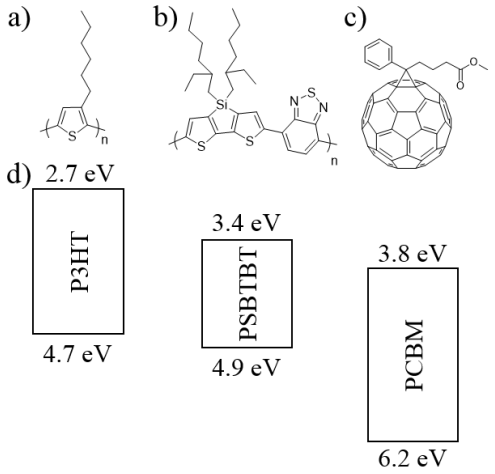

Fig. 1 Chemical structures of materials employed in this study: a) P3HT, b) PSBTBT, and c) PCBM. d) Energy levels of these three materials. The figures represent the HOMO (upper) and LUMO (lower) energy levels in electron volts. The details of the energy level evaluation are described in the Supplementary Information.

Experimental

Device fabrication

All devices were fabricated as follows: Indium–tin-oxide (ITO, 10 Ω per square) coated glass substrates were cleaned by ultrasonication in toluene, acetone, and ethanol for 15 min, dried with N_2, and then cleaned with a UV–O_3 cleaner for 30 min. A hole-transporting layer of poly(3,4-ethylenedioxythiophene) with poly(4-styrenesulfonate) (PEDOT:PSS, Celvios PH500) was spin-coated onto the cleaned substrates, and then dried at 140 °C for 10 min in air. Subsequently, the active layer was fabricated from a dichlorobenzene solution of P3HT (Plextronics, OS2000), PSBTBT (Solarmer Materials Inc.), and PCBM (Frontier Carbon, E100H) with different compositions. The solution was prepared with a blend ratio of P3HT : PSBTBT : PCBM = $10 - x : x$:10 mg mL^{-1} ($0 \le x \le 10$). For P3HT-H, the active layer was sipncoated at a spin rate of 600 rpm for 60 s and left in a Petri dish with a cover plate to evaporate the solvent slowly. Finally, a metal electrode of calcium (20 nm) and aluminium (100 nm) was thermally deposited in a vacuum (2.5 ×10^{-4} Pa) sequentially. For P3HT-L, the device was thermally annealed 140 °C for 5 min in a glove box (O_2 <10 ppm, H_2O <10 ppm).

Measurements

The *J–V* characteristics were measured in an N_2 atmosphere with a direct-current voltage/current source monitor (Advantest, R6243) in the dark and under illumination with AM1.5G simulated solar light at 100 mW cm^{-2}. The light intensity was corrected with a calibrated silicon photodiode reference cell (Bunkoh-Keiki, BS-520). The active area of the device was 0.07 cm^2. Absorption and PL spectra were measured with a spectrophotometer (Hitachi, U-3500) and a spectrofluorometer (Horiba Jobin Yvon, NanoLog) equipped with a calibrated imaging detector (Horiba Jobin Yvon, iHR320), respectively.

Results

Absorption spectra

Fig. 2 shows the absorption spectra of P3HT/PSBTBT/PCBM ternary blends with different blend compositions. As shown in the figure, two distinct absorption bands were observed at around 400–600 nm and 650–800 nm, which are ascribable to P3HT and PSBTBT, respectively. Because of complementary absorption bands, the ternary blends exhibit broad absorption bands ranging

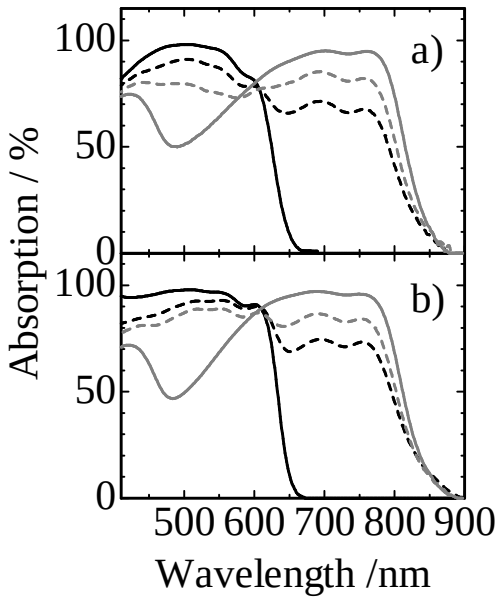

Fig. 2 Absorption spectra of ternary blend films covered with Al metal electrode, which was measured in the reflection mode. a) P3HT-L/PSBTBT/PCBM and b) P3HT-H/PSBTBT/PCBM with different blend ratios: P3HT : PSBTBT : PCBM = 50 : 0 : 50 (black solid lines), 30 : 20 : 50 (black broken lines), 20 : 30 : 50 (gray broken lines), and 0 : 50 : 50 (gray solid lines).

from 400 to 800 nm, which are desirable for the wide-band light harvesting in polymer solar cells. With increasing fraction of PSBTBT from 0 to 50 wt%, the PSBTBT absorption from 650 to 800 nm increased while the P3HT absorption from 400 to 600 nm decreased. For P3HT neat films, vibronic absorption bands were clearly observed at around 600 nm, which are ascribed to P3HT crystallization. On the basis of weakly interacting H-aggregated model,[61–64] the P3HT crystallinity is evaluated to be 50% for P3HT-L and 65% for P3HT-H. We note that these spectral changes can be reproduced by the sum of absorption spectra of P3HT and PSBTBT neat films. In other words, the P3HT crystallinity remained the same independently of the blend ratios.

Photoluminescence (PL) quenching

Fig. 3 shows the photoluminescence (PL) spectra of neat or blend films with different blend compositions. For P3HT-L/PSBTBT/PCBM ternary blend films, as shown in Fig. 3a, the PL from P3HT-L was strongly quenched with almost 100% quenching efficiency. For P3HT-L/PSBTBT binary blend films, the PL from P3HT was strongly quenched and instead the PL from PSBTBT was clearly observed, suggesting efficient energy transfer from P3HT to PSBTBT. From the spectral overlap, the Förster radius from P3HT to PSBTBT was estimated to be 3.5 nm assuming point-dipoles, which is long enough for the efficient energy transfer.[65] The PL from P3HT was completely quenched not only for P3HT-L/PSBTBT/PCBM ternary blends but also for P3HT-L/PCBM binary blends. In other words, almost 100% P3HT excitons are efficiently quenched mainly by PCBM in the presence or absence of PSBTBT. This is probably because PCBM molecules are well mixed with P3HT-L and hence can quench P3HT excitons efficiently in blend films. On the other hand, for P3HT-H/PSBTBT binary blend films, the PL from P3HT was strongly quenched and instead the PL from PSBTBT was clearly observed, again suggesting efficient energy transfer from P3HT to PSBTBT. For P3HT-H/PCBM binary blends, as shown in Fig. 3b, the PL from P3HT was quenched but still observed with 20% efficiency, indicating that 20% of P3HT excitons are radiatively deactivated to the ground state before arriving at the donor/acceptor interface. For P3HT-H/PSBTBT/PCBM ternary blends, the PL from P3HT was completely quenched. This is probably because the 20% P3HT excitons that would be lost in the absence of PSBTBT are collected to PSBTBT domains by energy transfer and then quenched by PCBM. These findings indicate that the charge generation efficiency is dependent upon the crystallinity of P3HT in ternary blend films.

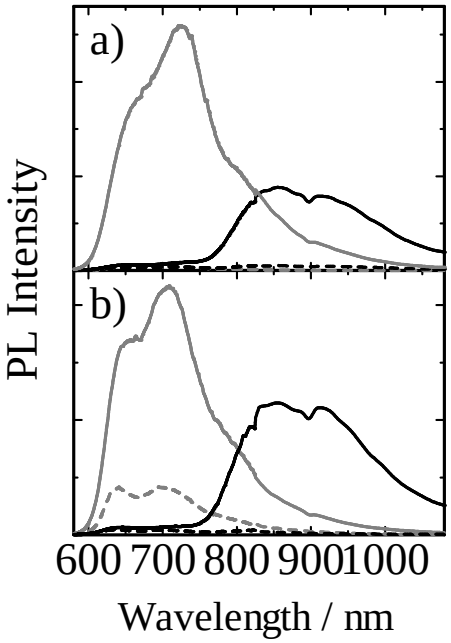

Fig. 3 PL spectra of a) P3HT-L and b) P3HT-H neat or blend films with different compositions: P3HT neat films (gray lines), P3HT/PCBM (50 : 50 w/w) (gray broken lines), P3HT/PSBTBT/PCBM (20 : 30 : 50 w/w) (broken lines), and P3HT/PSBTBT (40 : 60 w/w) (solid lines) blend films. The PL intensity of P3HT was corrected for variation in the absorption at an excitation wavelength of 550 nm. The PL intensity of PSBTBT was corrected by subtracting the PL intensity due to the direct excitation of PSBTBT at 550 nm.

***J–V* Characteristics**

Fig. 4 shows the *J–V* characteristics of P3HT/PSBTBT/PCBM ternary blend solar cells with different blend compositions. For

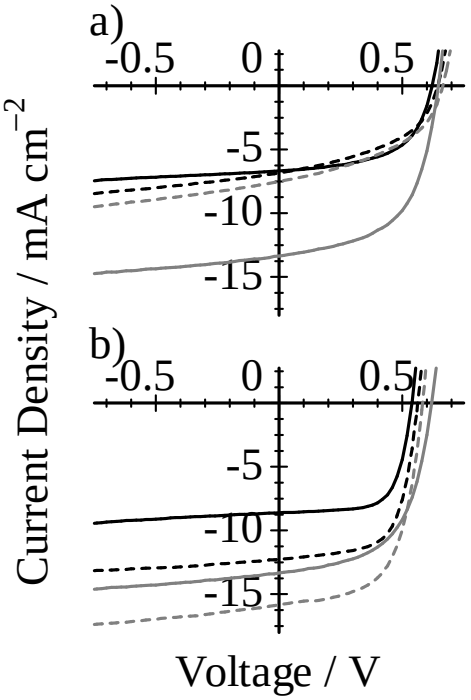

Fig. 4 *J–V* characteristics of a) P3HT-L/PSBTBT/PCBM and b) P3HT-H/PSBTBT/PCBM ternary solar cells with different blend compositions: P3HT : PSBTBT : PCBM = 50 : 0 : 50 (solid lines), 30 : 20 : 50 (broken lines), 20 : 30 : 50 (gray broken lines), and 0 : 50 : 50 (gray solid lines).

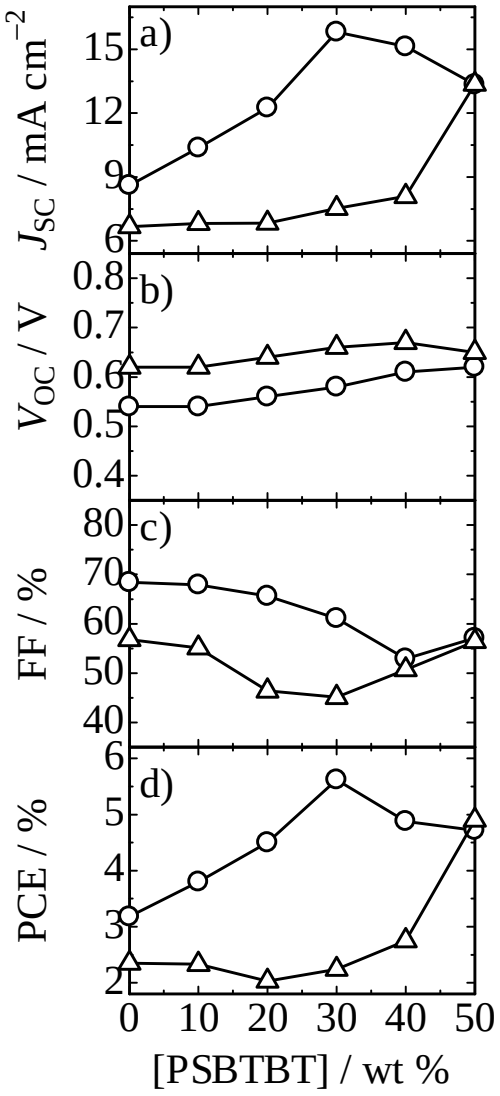

Fig. 5 Photovoltaic parameters plotted against the weight fraction of PSBTBT in ternary blend films: a) J_{SC}, b) V_{OC}, c) FF, and d) PCE. The open circles and triangles represent the photovoltaic parameters for ternary blends of P3HT-H/PSBTBT/PCBM and P3HT-L/PSBTBT/PCBM, respectively.

P3HT-L/PSBTBT/PCBM blends, as shown in Figs. 4a and 5, J_{SC} and V_{OC} increased only slightly and FF clearly decreased from 0.57 to 0.46 with increasing fraction of PSBTBT from 0 to 30 wt%, resulting in degraded PCE from 2.4 to 2.2%. At 50 wt% PSBTBT (PSBTBT/PCBM binary solar cell), J_{SC} jumped up to 13.4 mA cm^{-2} and FF recovered to 0.56, leading to the best PCE of 4.9%. A similar dependence has been reported previously for the same ternary blend solar cells.[44] In other words, the PCE of P3HT-L/PSBTBT/PCBM ternary blend solar cells is lower than that of PSBTBT/PCBM binary blend solar cells.

For P3HT-H/PSBTBT/PCBM blends, as shown in Fig. 4b, J_{SC} significantly increased from 8.6 to 15.8 mA cm^{-2} with increasing fraction of PSBTBT from 0 to 30 wt% and then decreased to 13.3 mA cm^{-2} at 50 wt% PSBTBT (PSBTBT/PCBM binary solar cell). On the other hand, no distinct changes in V_{OC} and FF were observed for all the blend compositions. Interestingly, the FF of ternary devices is even higher than that of the PSBTBT/PCBM binary reference device (0.57), suggesting that charge transport is better in ternary blends rather than in PSBTBT/PCBM binary blends. As a result, the best PCE of 5.6% was obtained for P3HT/PSBTBT/PCBM ternary blend solar cells (30 wt% PSBTBT). In other words, P3HT/PSBTBT/PCBM ternary blend solar cells exhibit higher PCE than either P3HT/PCBM or PSBTBT/PCBM binary blend solar cell.

External quantum efficiency (EQE)

Fig. 6 shows the EQE spectra of P3HT/PSBTBT/PCBM ternary blend solar cells with different blend compositions. For P3HT-L/PSBTBT/PCBM blends, as shown in Fig. 6a, the EQE signals at around 750 nm increased monotonically up to >60% while the EQE signals at around 500 nm decreased monotonically from ~50 to ~25% with increasing fraction of PSBTBT. This is consistent with the spectral change shown in Fig. 2a. For P3HT-H/PSBTBT/PCBM blends, on the other hand, the EQE signals at around 750 nm increased monotonically up to ~60% with increasing fraction of PSBTBT. As shown in Fig. 6b, this increase is much steeper than that observed for P3HT-L/PSBTBT/PCBM blends. Interestingly, the EQE signals at around 500 nm also increased from ~60 up to ~70% at 30 wt% PSBTBT even though the P3HT absorption decreased as shown in Fig. 2b, and then decreased to ~40% at 50 wt% PSBTBT (no P3HT). This is probably because efficient energy transfer from

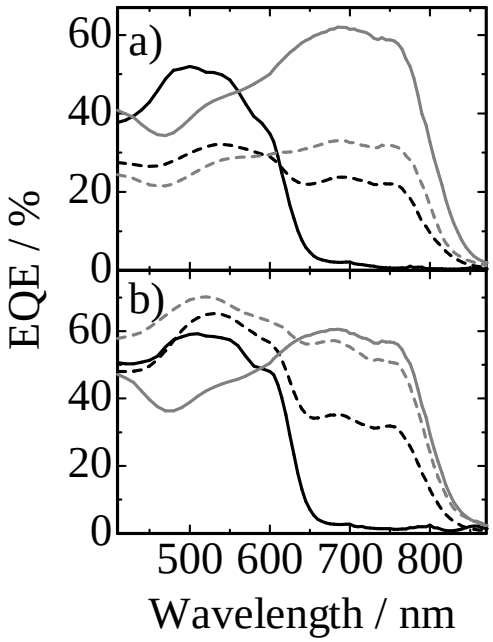

Fig. 6 EQE spectra of a) P3HT-L/PSBTBT/PCBM and b) P3HT-H/PSBTBT/PCBM ternary solar cells with different blend compositions: P3HT : PSBTBT : PCBM = 50 : 0 : 50 (solid lines), 30 : 20 : 50 (broken lines), 20 : 30 : 50 (gray broken lines), and 0 : 50 : 50 (gray solid lines).

P3HT to PSBTBT as we have shown recently.[65] Such energy transfer has been reported for dye-sensitized ternary blend polymer solar cells.[19,30,31,66] These findings suggest that the charge generation and transport mechanisms are dependent upon the crystallinity of P3HT in ternary blends.

Discussion

In order to address the origin of the difference in the photovoltaic performance between P3HT-L/PSBTBT/PCBM and P3HT-H/PSBTBT/PCBM ternary solar cells, we focus on the dependence of each photovoltaic parameter on the blend compositions. As shown in Fig. 5, remarkable differences were found in J_{SC} and PCE while no distinct difference was seen in V_{OC}. In particular, the composition dependence of PCE primarily follows that of J_{SC} for both ternary solar cells. In other words, the difference in the photovoltaic performance is primarily due to the difference in the J_{SC}. For P3HT-L/PSBTBT/PCBM, J_{SC} remains almost the same up to 30 wt% PSBTBT and jumps up at 50 wt% PSBTBT, resulting in almost the same PCE (~2%) up to 40 wt% PSBTBT and jumps to the most improved PCE (~5%) at 50 wt% PSBTBT. For P3HT-H/PSBTBT/PCBM, on the other hand, J_{SC} substantially increases up to 30 wt% PSBTBT and then slight decreases above 40 wt% PSBTBT, resulting the most improved PCE (5.6%) at 30 wt% PSBTBT, which is higher than that of either P3HT/PCBM or PSBTBT/PCBM binary blend solar cell.

First, we focus on the slight difference in the absorption spectra as shown in Fig. 2, which would cause the different dependence of J_{SC}. Here, we estimate the maximum contribution of each donor material to the photocurrent by integrating the product of their corresponding absorption spectra in the ternary blend, the sum of which corresponds to the maximum photocurrent. With increasing fraction of PSBTBT, as shown in Fig. 7, the increase in the photocurrent from PSBTBT exceeds the decrease in the photocurrent from P3HT, resulting in the increase in the maximum photocurrent up to more than 20 mA cm^{-2} for both ternary blend solar cells. Thus, the different dependence of J_{SC} cannot be ascribed to the slight difference in the photon absorption efficiency.

To discuss the different dependence of J_{SC} in more details, we estimate the contribution of each donor material to the photocurrent by integrating the product of their corresponding EQE spectra. For P3HT-L/PSBTBT/PCBM, as shown in Fig. 8a, the increase in the photocurrent from PSBTBT cancels out the decrease in the photocurrent from P3HT with increasing fraction

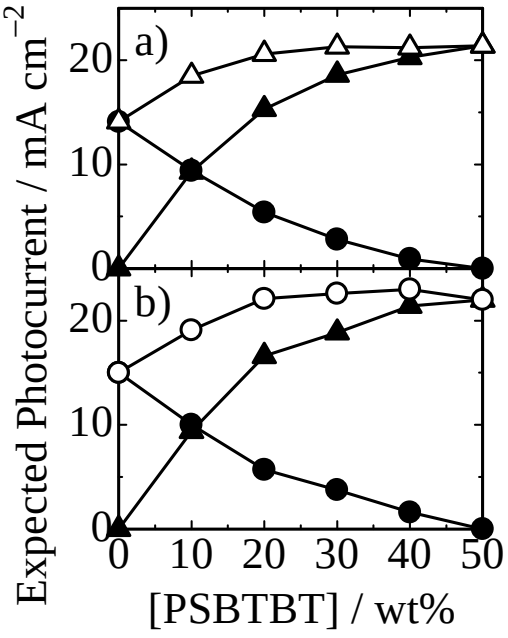

Fig. 7 Expected photocurrent of a) P3HT-L/PSBTBT/PCBM and b) P3HT-H/PSBTBT/PCBM ternary solar cells with different blend compositions, which is calculated from the absorption and AM1.5G solar spectra under the assumption that all the absorbed photons are converted to current. The closed circles represent photocurrent from P3HT, and the closed triangles represent photocurrent from PSBTBT, the open triangles and open circle represent the sum of the photocurrent from P3HT (closed circles) and from PSBTBT (triangles), respectively, which correspond to the maximum photocurrent J_{max} with IQE = 100%.

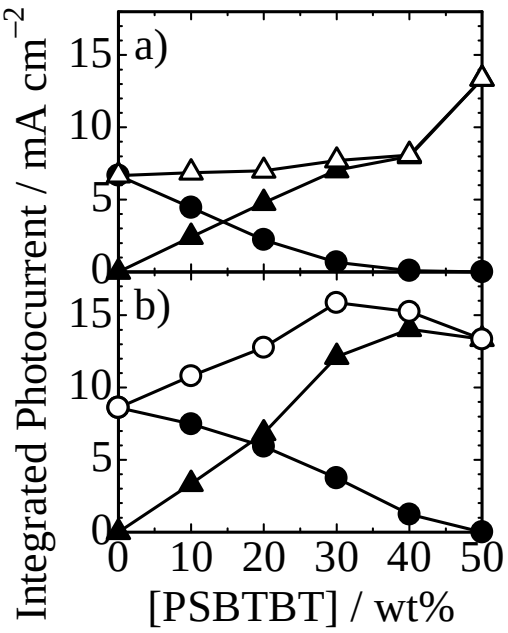

Fig. 8 Integrated photocurrent of a) P3HT-L/PSBTBT/PCBM and b) P3HT-H/PSBTBT/PCBM ternary solar cells with different blend compositions, which is calculated from the EQE and AM1.5G solar spectra. The closed circles represent photocurrent from P3HT, the closed triangles represent photocurrent from PSBTBT, the open triangles and open circle represent the sum of the photocurrent from P3HT (closed circles) and from PSBTBT (triangles), respectively, which correspond to the total photocurrent J_{SC}.

of PSBTBT in the ternary blends, resulting in the almost constant total photocurrent (J_{SC}) up to 40 wt% PSBTBT. For P3HT-H/PSBTBT/PCBM, as shown in Fig. 8b, the photocurrent from PSBTBT increases more steeply and the photocurrent from P3HT decreases more gradually with increasing fraction of PSBTBT. As a result, the total photocurrent (J_{SC}) shows the maximum at 30 wt% PSBTBT. As mentioned above, this improvement in J_{SC} cannot be ascribed to the photon absorption efficiency but rather should be ascribed to the charge generation or charge collection efficiency. The enhanced photocurrent from P3HT in P3HT-H/PSBTBT/PCBM is partly ascribed to the improved charge generation due to energy transfer from P3HT to PSBTBT as described before, which can harvest P3HT excitons that would be lost in the absence of PSBTBT. On the other hand, the enhanced photocurrent from PSBTBT is most probably due to the improved charge collection in the presence of P3HT because FF remains as high as >0.6 up to 30 wt% PSBTBT as shown in Fig. 5.

Finally, we propose the photovoltaic conversion mechanism in P3HT-H/PSBTBT/PCBM ternary solar cells as shown in Scheme 1. Because of the high crystallinity of P3HT-H, there are at least four phases in ternary blends: P3HT crystalline phase, P3HT amorphous phase mixed with PCBM, PSBTBT phase mixed with PCBM, and PCBM rich phase. Although PSBTBT is also a crystalline polymer, it is considered to be one phase because PSBTBT crystallites are so small that the exciton diffusion is negligible as reported previously.[67] Upon the photoexcitation of P3HT, P3HT excitons generated near the interface or in the amorphous domains are promptly converted to P3HT polarons and P3HT excitons generated in the large crystalline domains are collected to PSBTBT domains by energy transfer, which would be lost in the absence of PSBTBT. As reported previously, some P3HT polarons are transferred to more stable crystalline domains because of smaller ionization potential.[68] Upon the photoexcitation of PSBTBT, PSBTBT excitons are promptly converted to PSBTBT polarons, some of which would be transferred to more stable P3HT crystalline domains. Indeed, we have shown that PSBTBT polarons are transferred from disordered to crystalline domains in PSBTBT/PCBM blends.[67] In summary, the improved PCE is most probably because of the energy transfer from P3HT to PSBTBT and the efficient charge transport due to crystalline P3HT. In other words, crystalline wide-bandgap polymer and amorphous low-bandgap polymer would be suitable combination for ternary blend solar cells.

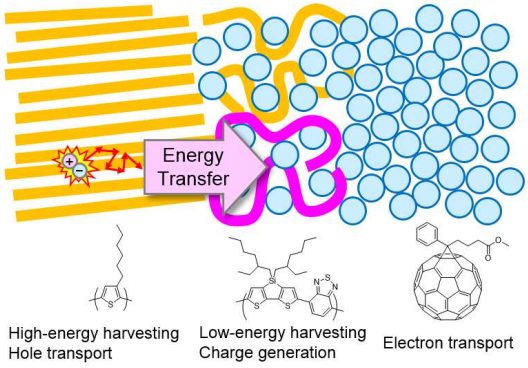

Scheme 1 Schematic illustration of exciton diffusion followed by energy transfer from P3HT to PSBTBT in P3HT-H/PSBTBT/PCBM ternary blends which consists of P3HT crystalline phase (left), P3HT amorphous phase mixed with PCBM (upper middle), PSBTBT phase mixed with PCBM (bottom middle), and PCBM rich phase (right).

Conclusion

In summary, we demonstrated that the photovoltaic performance of P3HT/PSBTBT/PCBM ternary solar cells can be effectively improved by using highly crystalline P3HT. This is because highly crystalline P3HT forms large crystalline domains and hence would improve charge transport even in ternary blends. Even in such large P3HT crystalline domains, P3HT excitons are effectively collected by energy transfer to PSBTBT domains mixed with PCBM where charge carriers are efficiently generated. This is because of the large spectral overlap between the P3HT fluorescence and the PSBTBT absorption. As a result, J_{SC} was improved to 15.8 mA cm^{-2} with a high fill factor of 0.61 at a weight ratio of P3HT : PSBTBT : PCBM = 20 : 30 : 50, and hence PCE reached 5.6%, which is even higher than that of both individual binary solar cells based on P3HT/PCBM and PSBTBT/PCBM reported so far. We believe that this finding is generally applicable to other ternary blend polymer solar cells. We propose that a wide-bandgap crystalline polymer and a low-bandgap amorphous polymer would be good combination for highly efficient ternary solar cells. Because of large spectral overlap between the wide-bandgap polymer fluorescence and the low-bandgap polymer absorption, excitons even in large crystalline domains of the wide-bandgap polymer are efficiently harvested by energy transfer to the low-bandgap polymer domains mixed with PCBM followed by prompt charge generation. Most of charge carriers are likely to be transferred to more stable crystalline domains of the wide-bandgap polymer where charge transport would be efficient.

Acknowledgements

This work was partly supported by the FIRST program (Development of Organic Photovoltaics toward a Low-Carbon Society: Pioneering Next Generation Solar Cell Technologies and Industries via Multi-manufacturer Cooperation), the JST PRESTO program (Photoenergy Conversion Systems and Materials for the Next Generation Solar Cells), the JST CREST program (Phase Interfaces for Highly Efficient Energy Utilization), and the JST Advanced Low Carbon Technology Research and Development (ALCA) program.

Notes and references

[a] Department of Polymer Chemistry, Graduate School of Engineering, Kyoto University, Katsura, Nishikyo, Kyoto 615-8510, Japan.
[b] Present address: School of Materials Science and Engineering, Changzhou University, Changzhou 213164, PR China.
[c] Japan Science and Technology Agency (JST), PRESTO, 4-1-8 Honcho Kawaguchi, Saitama 332-0012, Japan.

1. K. A. Mazzio and C. K. Luscombe, *Chem. Soc. Rev.*, 2015, **44**, 78–90.
2. J. Yu, Y. Zheng, and J. Huang, *Polymer*, 2014, **6**, 2473–2509.
3. M. C. Scharber and N. S. Sariciftci, *Prog. Polym. Sci.*, 2013, **38**, 1929–1940.
4. N. Yeh and P. Yeh, *Renew. Sus. Energy Rev.*, 2013, **21**, 421-431.
5. L. Dou, J. B. You , Z. R. Hong , Z. Xu , G. Li, R. A. Street , and Y. Yang, *Adv. Mater.*, 2013, **25**, 6642–6671.
6. M. A. Green1, K. Emery, Y. Hishikawa, W. Warta, and E. D. Dunlop, *Prog. Photovolt: Res. Appl.*, 2015, **23**, 805–812.
7. S. H. Liao, H. J. Jhuo, P. N. Yeh, Y. S. Cheng, Y. L. Li, Y. H. Lee, S. Sharma, and S. A. Chen, *Sci. Rep.*, 2014, **4**, 6813.
8. Y. Liu, J. Zhao, Z. Li, C. Mu, W. Ma, H. Hu, K. Jiang, H. Lin, H. Ade, and H. Yan, *Nat. Commun.*, 2014, **5**, 5293.
9. J. D. Chen, C. Cui, Y. Q. Li, L. Zhou, Q. D. Ou, C. Li, Y. Li, and J. X. Tang, *Adv. Mater.*, 2015, **27**, 1035–1041.
10. Z. He, B. Xiao, F. Liu, H. Wu, Y. Yang, S. Xiao, C. Wang, T. P. Russell, and Y. Cao, *Nat. Photonics*, 2015, **9**, 174–179.
11. E. Bundgaard and F. C. Krebs, *Sol. Energy Mater. Sol. Cells*, 2007, **91**, 954–985.
12. W. L. Ma, C. Y. Yang, X. Gong, K. Lee, and A. J. Heeger, *Adv. Funct. Mater.*, 2005, **15**, 1617–1622.
13. Y. Kim, S. Cook, S. Tuladha, S. A. Choulis, J. Nelson, J. R. Durrant, D. D. C. Bradley, M. Giles, I. McCulloch, C.-S. Ha, and M. Ree, *Nat. Mater.*, 2006, **5**, 197–203.
14. T. Ameri, P. Khoram, J. Min, and C. J. Brabec, *Adv. Mater.*, 2013, **25**, 4245–4266.
15. L. Yang, L. Yan, and W. You, *J. Phys. Chem. Lett.*, 2013, **4**, 1802–1810.
16. Y. C. Chen, C. Y. Hsu, R. Y. Y. Lin, K. C. Ho, and J. T. Lin, *ChemSusChem*, 2013, **6**, 20–35.
17. F. Goubard and G. Wantz, *Polym. Int.*, 2014, **63**, 1362–1367.
18. B. M. Savoie, S. Dunaisky, T. J. Marks, and M. A. Ratner, *Adv. Energy Mater.*, 2015, **5**, 1400891.
19. Y. Wang, H. Ohkita, H. Benten, and S. Ito, *Trans. Mater. Res. Soc. Jpn.*, 2014, **39**, 439–442.
20. J. Zhang, Y. Zhang, J. Fang, K. Lu, Z. Wang, W. Ma, and Z. Wei, *J. Am. Chem. Soc.*, 2015, **137**, 8176–8183.
21. H. Xu, T. Wada, H. Ohkita, H. Benten, and S. Ito, *Sci. Rep.*, 2015, **5**, 9321.
22. B. Lim, J. T. Bloking, A. Ponec, M. D. McGehee, and A. Sellinger, *ACS Appl. Mater. Interfaces*, 2014, **6**, 6905–6913.
23. H. Xu, H. Ohkita, T. Hirata, H. Benten, and S. Ito, *Polymer*, 2014, **55**, 2856–2860.
24. A. Kokil, A. M. Poe, Y. Bae, A. M. D. Pelle, P. J. Homnick, P. M. Lahti, J. Kumar, and S. Thayumanavan, *ACS Appl. Mater. Interfaces*, 2014, **6**, 9920–9924.
25. Y. Wang, B. Zheng, Y. Tamai, H. Ohkita, H. Benten, and S. Ito, *J. Electrochem. Soc.*, 2014, **161**, D3093–D3096.
26. H. Xu, T. Wada, H. Ohkita, H. Benten, and S. Ito, *Electrochim. Acta*, 2013, **100**, 214–219.
27. X. Xiao, G. Wei, S. Wang, J. D. Zimmerman, C. K. Renshaw, M. E. Thompson, and S. R. Forrest, *Adv. Mater.*, 2012, **24**, 1956–1960.
28. S. Honda, H. Ohkita, H. Benten, and S. Ito, *Adv. Energy Mater.*, 2011, **1**, 588–598.
29. Z. X. Xu, V. A. L. Roy, K. H. Low, and C. M. Che, *Chem. Commun.*, 2011, **47**, 9654–9656.
30. S. Honda, H. Ohkita, H. Benten, and S. Ito, *Chem. Commun.*, 2010, **46**, 6596–6598.
31. S. Honda, T. Nogami, H. Ohkita, H. Benten, and CAS. Ito, *ACS Appl. Mater. Interfaces*, 2009, **1**, 804–810.
32. J. Peet, A. B. Tamayo, X. D. Dang, J. H. Seo, and T. Q. Nguyen, *Appl. Phys. Lett.*, 2008, **93**, 163306.
33. Y. M. Yang, W. Chen, L. Dou, W. H. Chang, H. S. Duan, B. Bob, Gang, Li, and Y. Yang, *Nat. Photonics*, 2015, **9**, 190–198.
34. S. Liu, P. You, J. Li, J. Li, C. S. Lee, B. S. Ong, C. Surya, and F. Yan, *Energy Environ. Sci.*, 2015, **8**, 1463–1470.
35. H. Lu, X. Zhang, C. Li, H. Wei, Q. Liu, W. Li, and Z. Bo, *Macromol. Rapid Commun.*, 2015, **36**, 1348–1353.
36. L. Lu, W. Chen, T. Xu, and L. Yu, *Nat. Commun.*, 2015, **6**, 7327.
37. P. Cheng, Y. Li, and X. Zhan, *Energy Environ. Sci.*, 2014, **7**, 2005–2011.
38. H. Yan, D. Li, Y. Zhang, Y. Yang, and Z. Wei, *J. Phys. Chem. C*, 2014, **118**, 10552–10559.
39. Y. Gu, C. Wang, F. Liu, J. Chen, O. E. Dyck, G. Duscherd, and T. P. Russell, *Energy Environ. Sci.*, 2014, **7**, 3782–3790.
40. R. Lin, M. Wright, K. H. Chan, B. P. Veettil, R. Sheng, X. Wen, and A. Uddin, *Org. Electron.*, 2014, **15**, 2837–2846.
41. L. Lu, T. Xu, W. Chen, E. S. Landry, and Luping Yu, *Nat. Photonics*, 2014, **8**, 716–722.
42. T. Ameri, T. Heumuller, J. Min, N. Li, G. Matt, U. Scherf, and C. J. Brabec, *Energy Environ. Sci.*, 2013, **6**, 1796–1801.
43. Q. An, F. Zhang, J. Zhang, W. Tang, Z. Wang, L. Li, Z. Xu, F. Teng, and Y. Wang, *Sol. Energy Mater. Sol. Cells*, 2013, **118**, 30–35.
44. T. Ameri, J. Min, N. Li , F. Machui, D. Baran, M. Forster, K. J. Schottler, D. Dolfen, U. Scherf, and C. J. Brabec, *Adv. Energy Mater.*, 2012, **2**, 1198–1202.
45. Z. Hu, S. Tang, A. Ahlvers, S. I. Khondaker, and A. J. Gesquiere, *Appl. Phys. Lett.*, 2012, **101**, 053308.
46. J. M. Lobez, T. L. Andrew, V. Bulovic, and T. M. Swager, *ACS Nano*, 2012, **6**, 3044–3056.
47. P. P. Khlyabich, B. Burkhart, and B. C. Thompson, *J. Am. Chem. Soc.*, 2012, **134**, 9074–9077.
48. L. Yang, H. Zhou, S. C. Price, and W. You, *J. Am. Chem. Soc.*, 2012, **134**, 5432–5435.

49. M. C. Chen, D. J. Liaw, Y. C. Huang, H. Y. Wu, and Y. Tai, *Sol. Energy Mater. Sol. Cells*, 2011, **95**, 2621–2627.
50. G. Adam, A. Pivrikas, A. M. Ramil, S. Tadesse, T. Yohannes, N. S. Sariciftci, and D. A. M. Egbe, *J. Mater. Chem.*, 2011, **21**, 2594–2600.
51. M. Koppe, H. J. Egelhaaf, G. Dennler, M. C. Scharber, C. J. Brabec, P. Schilinsky, and C. N. Hoth, *Adv. Funct. Mater.*, 2010, **20**, 338–346.
52. M. Shin, H. Kim, S. Nam, J. Park, and Y. Kim, *Energy Environ. Sci.*, 2010, **3**, 1538–1543.
53. H. Kim, M. Shin, and Y. Kim, *J. Phys. Chem. C*, 2009, **113**, 1620–1623.
54. H. Lu, B. Akgun, and T. P. Russell, *Adv. Energy Mater.*, 2011, **1**, 870–878.
55. H. Y. Chen, J. Hou, A. E. Hayden, H. Yang, K. N. Houk, and Y. Yang, *Adv. Mater.*, 2010, **22**, 371–375.
56. H. Y. Chen, J. Hou, S. Zhang, Y. Liang, G. Yang, Y. Yang, L. Yu, Y. Wu, and G. Li, *Nat. Photonics*, 2009, **3**, 649–653.
57. Z. He, C. Zhong, S. Su, M. Xu, H. Wu, and Y. Cao, *Nat. Photonics*, 2012, **6**, 591–595.
58. J. Peet, J. Y. Kim, N. E. Coates, W. L. Ma, D. Moses, A. J. Heeger, and G. C. Bazan, *Nat. Mater.*, 2007, **6**, 497–500.
59. M. Koppe, H. J. Egelhaaf, E. Clodic, M. Morana, L. Luer, A. Troeger, V. Sgobba, D. M. Guldi, T. Ameri, and C. J. Brabec, *Adv. Energy Mater.*, 2013, **3**, 949–958.
60. J. Hou, H. Y. Chen, S. Zhang, G. Li, and Y. Yang, *J. Am. Chem. Soc.*, 2008, **130**, 16144–16145.
61. Y. Tamai, Y. Matsuura, H. Ohkita, H. Benten, and S. Ito, *J. Phys. Chem. Lett.*, 2014, **5**, 399–403.
62. F. C. Spano, *J. Chem. Phys.*, 2005, **122**, 234701.
63. F. C. Spano, *Chem. Phys.*, 2006, **325**, 22–35.
64. J. Clark, J. F. Chang, F. C. Spano, R. H. Friend, and C. Silva, *Appl. Phys. Lett.*, 2009, **94**, 163306.
65. Y. Wang, H. Ohkita, H. Benten, and S. Ito, *ChemPhysChem*, 2015, **16**, 1263–1267.
66. S. Honda, S. Yokoya, H. Ohkita, H. Benten, and S. Ito, *J. Phys. Chem. C*, 2011, **115**, 11306–11317.
67. Y. Tamai, K. Tsuda, H. Ohkita, H. Benten, and S. Ito, *Phys. Chem. Chem. Phys.*, 2014, **16**, 20338–20346.
68. J. Guo, H. Ohkita, H. Benten, and S. Ito, *J. Am. Chem. Soc.*, 2010, **132**, 6154–6164.

Graphical Abstract

Ternary blend solar cells using a crystalline wide-bandgap P3HT and a low-bandgap PSBTBT exhibit good exciton harvesting and charge transport.